JOURNAL OF COMPUTATIONAL PHYSICS 50, 38–70 (1983)

A Baroclinic Quasigeostrophic Open Ocean Model

ROBERT N. MILLER, ALLAN R. ROBINSON, AND DALE B. HAIDVOGEL

Division of Applied Sciences, Harvard University, Cambridge, Massachusetts 02138

Received October 28, 1981

A baroclinic quasigeostrophic open ocean model is presented, calibrated by a series of test problems, and demonstrated to be feasible and efficient for application to realistic mid-oceanic mesoscale eddy flow regimes. Two methods of treating the depth dependence of the flow, a finite difference method and a collocation method, are tested and intercompared. Sample Rossby wave calculations with and without advection are performed with constant stratification and two levels of nonlinearity, one weaker than and one typical of real ocean flows. Using exact analytical solutions for comparison, the accuracy and efficiency of the model is tabulated as a function of the computational parameters and stability limits set; typically, errors were controlled between 1% and 10% RMS after two wave periods. Further Rossby wave tests with realistic stratification and wave parameters chosen to mimic real ocean conditions were performed to determine computational parameters for use with real and simulated data. Finally, a prototype calculation with quasiturbulent simulated data was performed successfully, which demonstrates the practicality of the model for scientific use.

1. INTRODUCTION

Models of oceanic mesoscale processes have played, and will continue to play, a key role in our understanding of mid-ocean dynamics. (See, e.g., [7]). Oceanic mesoscale variability is generally defined as variability on spatial scales of tens to hundreds of kilometers, and on temporal scales from weeks to months. Motions on this scale are the oceanic analogue of weather—the dynamic analogue of the atmospheric "synoptic" scale. The circulatory systems that correspond to the familiar highs and lows in meteorology are the mesoscale eddies. For mid-ocean eddies, intensive composite data sets have been constructed from observations taken during the 1970s by the large experimental program MODE [14] and POLYMODE [20].

A model with open boundary conditions is required for forecast studies with real data and for idealized numerical experiments to investigate importation of energy and scales from remote regions. The development of a barotropic open ocean model by the Harvard Open Ocean Modeling Group was reported in [8], in which problems of open ocean modeling of mesoscale currents were discussed in a broader context. The results of dynamical forecast experiments with this model are reported by Robinson and Haidvogel [22] who also present a detailed discussion of the philosophy of limited area modeling of the oceanic mesoscale. Real ocean flows are known to be significantly baroclinic; statistically, the ratio of barotropic to baroclinic kinetic

0021-9991/83 $3.00

energy has been estimated at approximately 0.5 [11]. This paper concerns the extension of the earlier barotropic modeling work to a baroclinic quasigeostrophic forecast model. With this step, the model becomes capable of direct application to the analysis of the MODE/POLYMODE data base, and to other such data sets available now or in the future in arbitrary open ocean regions.

Other baroclinic eddy-resolving models have been developed during the past ten years. Robinson *et al.* [21] present a review of the basin and large scale general circulation models, including those with sufficiently fine resolution to reveal mesoscale processes. Such models are known as eddy-resolving general circulation models (EGCMs). Haidvogel [7] discusses the so-called process or regional models, which are most suitable for the dynamic analysis of intensive data sets. Bretherton and Karweit [3] have constructed a baroclinic model with periodic boundary conditions for process studies to the MODE data [18], which was subsequently applied to important studies of dynamic balances related to the design and analysis of aspects of POLYMODE [17]. The imposition of periodic boundary conditions limits this type of model essentially to statistical comparisons.

Regional ocean models with open boundary conditions are now being used in universities and laboratories in the U.S. and U.S.S.R. for the analysis of the MODE and POLYMODE data sets and for related dynamical process studies. These studies are also at the forefront of applied research for practical regional ocean forecasting which is of importance for naval operations and commercial purposes [16]. Additionally, the results of these studies contribute to our understanding of the dispersal of tracer material naturally occuring in the ocean or present as a pollutant, such as that which could emanate from nuclear waste dumping sites [10]. Such studies are also important in the oceanographic interpretation of satellite data and generally in the planning of observational strategies. Since this version of the model is the one that will be used for these scientific purposes, systematic quantitative determination of modeling characteristics is necessary for proper interpretation of modeling results. The purpose of this study is to document the quantitative behavior of this model in parameter ranges of interest.

Here we report in detail the testing and calibration of our baroclinic model, i.e., the establishment of the computational characteristics of the model as determined by its application to a series of idealized quasigeostrophic flow problems. Computational parameters were chosen to be consistent with our most detailed knowledge of actual conditions in the ocean. The characteristics of the baroclinic model are similar in broad outline to the barotropic results, but the quantitative differences reflect the inclusion of baroclinic physics.

The problems we chose for the evaluation of model characteristics are predominantly Rossby wave propagation with and without advection in the presence of stratification (imposed either as uniform or with an oceanically realistic structure). Since exact solutions for these waves are available, these provide the basis for the quantification of the computational error properties of the model. Finally, we present a test of the model for a flow field which is of the nonlinear and quasiturbulent type more characteristic of the real ocean; this problem involves a test region embedded in

TABLE Ii

Rossby Waves, Constant Stratification

Run #	Mode	Levels	τ	ε	Advect	Filter ord–freq	Bottom friction	Angle	Method	Duration (periods)	Ending errors top level RMS ψ'	Ending errors top level RMS ζ'
1	0	4	64	0.4	0	0–0	0	0.5932	—	2	0.012	0.026
2	1	2	64	0.4	0	0–0	0	0.5932	FD	2	0.27	0.26
									COLL	2	0.012	0.026
3	1	4	64	0.4	0	0–0	0	0.5932	FD	2	0.078	0.076
									COLL	2	0.014	0.024
4	1	8	64	0.4	0	0–0	0	0.5932	FD	2	0.029	0.033
5	1	2	64	0.4	0	0–0	0	2.164	FD	2	0.16	0.28
6	1	4	64	0.4	0	0–0	0	2.164	FD	2	0.046	0.079
									COLL	2	0.0097	0.0253
6a	1	4	32	0.4	0	0–0	0	0.5932	COLL	2	0.038	0.045
7	1	4	64	0.4	0.5	0–0	0	0.5932	FD	2	0.034	0.090
									COLL	2	0.003	0.026
8	1	4	64	0.4	0.5	0–0	0	2.164	FD	2	0.02	0.091
									COLL	2	0.0030	0.025
9	2	4	64	0.4	0	4–1	0	0.5932	FD	2	0.73	0.83
						0–0			COLL	2	0.015	0.030
10	2	8	64	0.4	0	0–0	0	0.5932	FD	2	0.18	0.21
11	2	4	64	0.4	0.5	0–0	0	0.5932	FD	2	0.37	1.3
									COLL	2	0.0037	0.035
12	3	4	128	0.4	0	2–1	0	0.5932	FD	2	2.14	1.51
			64	0.4	0	0–0	0	0.5932	COLL	2	0.019	0.033
13	1	4	64	1.5	0	0–0	0	0.5932	FD	2	0.16	5.4
14	1	4	64	1.5	0.2	2–1	0	0.5932	FD	2	0.182	0.267
									COLL	2	0.125	0.179
15	1	4	64	1.5	0.2	2–1	0.016	0.5932	FD	2	0.451	0.64
									COLL	2	0.409	0.576
16	1	4	64	1.5	0.2	2–1	0.032	0.5932	COLL	2	0.596	0.846
17	1	4	64	1.5	0.2	2–2	0	0.5932	COLL	2	0.068	0.100
	1	4	64	1.5	0.2	2–2	0	0.5932	FD	2	0.158	0.235

a larger simulated flow according to the strategy presented in [22]. These results establish the model as efficient and feasible for application to real ocean mesoscale studies, and the accuracy characteristics tabulated provide the basis for initial choices of computational parameters in such studies.

The matrix of tests performed for the calibration of the baroclinic model is shown in Table Ii–Iii. Runs 1–17 in Table Ii show the comparison between two methods of treating the depth dependence of the flow; a finite difference method and a collocation method. The methods are compared at low and moderate levels of nonlinearity (details below), with lateral resolution fixed and stratification parameters held constant at values typical of the main thermocline. Rossby waves with and without advection for two different propagation directions are used as examples to test two methods. Our tests show that the finite difference method required more vertical resolution than the collocation method to achieve comparable accuracy, and the disparity in computational efficiency becomes greater at higher baroclinic modes. Runs 18–28 in Table Iii show the results of a series of Rossby wave tests designed to investigate the capabilties of the model in parameter ranges appropriate to real ocean data. Vertical stratification structure is taken from the MODE data [15]. Rossby wave parameters are chosen to simulate the magnitude of the nonlinear terms in real data. Lateral resolution is held constant at a level determined by earlier experience [8, 22]. Temporal resolution was varied in order to determine error control and stability requirements in several flow regimes. Finally, runs 29 and 30 show the preliminary results from the construction of a model forecast data set from the four best fit Rossby waves to the MODE-I data [13, 22]. In the earlier barotropic data set, the two barotropic waves from the MODE fit are used to initialize the model on a 1000×1000 km domain, upon which a uniform 65×65 grid was imposed. The data set is then generated by the nonlinear interaction of these waves. The baroclinic data set is generated in analogous fashion on a domain of 5 km depth and of the same lateral extent and resolution as the barotropic simulated data set. The baroclinic simulation could not be stabilized with the one day time steps that were used in the barotropic simulation; six hour time steps, 256 steps per half period, were used in the baroclinic simulation.

This data set will be used for testing and calibration of dynamical, statistical, and mixed statistical/dynamical forecasting techniques. Here we display a successful prototype baroclinic interior calculation similar to those reported in [22] using the interior $500 \times 500 \times 5$ km region of the simulated data set to provide boundary and initial conditions for a computation using a $33 \times 33 \times 6$ grid. Computations were performed on the GLAS Amdahl 470. On that machine, each step of our Rossby wave simulation on a 33×33 lateral grid requires approximately $\frac{1}{2}$ second of CPU time per vertical level.

TABLE Iii

Single Rossby Wave Tests with Realistic Stratification

Run #	ε	γ	Δt	RMS max $\Delta\psi$	min $\Delta\psi$	RMS max $\Delta\zeta$	min $\Delta\zeta$	Duration	Filter	$\varepsilon k\gamma$	τ	Vertical structure[a]
18	4.0	0.5	0.0865 (=1 day)	0.191	0.092	3.99	0.543	48 days	2–1	1.66	27.8	USSR PM
19	4.0	0.5	0.0432	0.009	0.004	0.100	0.053	60 days	2–1	1.66	55.6	USSR PM
20	4.0	0.5	0.0432	0.008	0.0006	0.053	0.051	60 days	2–1	1.66	55.6	4 levels optimal
21	4.0	0.5	0.0432	0.009	0.001	0.057	0.051	60 days	2–1	1.66	55.6	6 levels optimal
22	4.0	0.5	0.0432	0.005	0.0007	0.037	0.032	60 days	2–2	1.66	55.6	6 levels optimal
23	4.0	0.5	0.0216	0.009	0.004	0.100	0.053	60 days	2–2	1.66	111.3	USSR PM
24	5.9	0.01	0.0865	0.245	0.037	0.165	0.045	60 days	2–1	0.049	119.6	USSR PM
25	5.9	0.01	0.0432	0.234	0.036	0.158	0.044	60 days	2–2	0.049	239.2	USSR PM
26	5.9	0.01	0.0432	0.347	0.060	0.228	0.076	60 days	2–1	0.049	239.2	USSR PM
27	1.5	4.0	0.0432	0.173	0.060	55.4	43.2	20 days	2–1	4.97	15.71	USSR PM
28	1.5	4.0	0.0216	0.0006	0.0001	0.234	0.145	60 days	2–2	4.97	31.42	USSR PM

Prototype calculation with simulated data

Run #	ε	Δt	x_B	Filter	Vertical structure	Duration	Remarks
29	1.48	0.0118	36.744	4–2–1	200, 420, 750, 1020, 2110, 3600 m	704 days	exterior calculation
30	1.48	0.0118	18.372	4–2–1	200, 420, 750, 1020, 2110, 3600 m	64 days	interior calculation beginning at day 16

[a] Vertical structure notation: USSR PM = 100, 400, 700, 1400 meters; 4 levels optimal = 200, 700, 1300, 3330 meters; 6 levels optimal = 100, 400, 800, 1100, 2150, 3720 meters.

2. Modeling Equations and Methods

2.1 *The Quasigeostrophic Model*

As in the barotropic case, we nondimensionalize x, y, t, and ψ by d, d, $(\beta d)^{-1}$, and $(V_0 d)$, respectively. The parameters d and V_0 represent characteristic length and velocity scales of the anticipated field of motion. The length scale d does not correspond to the basin size L. The nondimensional basin size $x_B = L/d$ is in general greater than one. Here β is the conventional linearized variation of planetary vorticity with latitude. We introduce the scale depth h_T, which, in our simulations of real ocean conditions, represents the depth of the main thermocline. We use this depth to nondimensionalize the vertical coordinate z, measured positive upward. We distinguish h_T from the total depth L_z, though, in our first series of experiments, we choose the scale depth equal to the total depth. The nondimensional total depth of our model region is $H = L_z/h_T$, which is, in general, greater than one. In this scaling, we write the baroclinic quasigeostrophic model equation as follows:

$$\left(\frac{\partial}{\partial t} + \varepsilon \mathcal{J}(\psi, \cdot)\right)\zeta + \psi_x = \mathcal{F}, \tag{1}$$

$$\nabla^2 \psi + \Gamma^2(\sigma\psi_z)_z = \zeta. \tag{2}$$

As in the barotropic model, ε is the β–Rossby number $V_0/\beta d^2$.

In this baroclinic formulation, we introduce the parameters Γ^2 and σ which describe the stratification of our model region. These parameters are defined as follows:

$$\Gamma^2 = f_0^2 d^2/(N_0^2 h_T^2),$$

where

N_0 is a characteristic buoyancy frequency;

f_0 is the coriolis parameter at the center of the basin;

d and h_T are as defined above;

$\sigma(z) = N_0^2/N^2(z)$, where $N^2(z) = -(g/\rho_0)(\partial\rho(z)/\partial z)$ is the buoyancy frequency as a function of depth, ρ_0 is the mean density, and $\rho(z)$ is the vertical profile of density averaged in time and in the horizontal.

The quasigeostrophic streamfunction relates in the conventional way to the velocity components and the pressure:

$$u = -\psi_y, \qquad v = \psi_x, \qquad p = \rho_0 f_0 \psi.$$

The density anomaly δ, loosely referred to as the "temperature anomaly," is given in terms of the quasigeostrophic streamfunction as

$$\delta = \Gamma^2 \sigma \psi_z.$$

TABLE II[a]

Response Frequency of a Shapiro Filter of Order n and Frequency m

Frequency	Order			Wavelength in gridpoint units
	1	2	4	
1	0.0000	0.0000	0.0000	2
	0.5000	0.7500	0.9375	4
	0.7500	0.9375	0.9961	6
	0.9330	0.9955	1.0000	12
2	0.0000	0.0000	0.0000	2
	0.2500	0.5625	0.8789	4
	0.5625	0.8789	0.9922	6
	0.8705	0.9910	1.0000	12
4	0.0000	0.0000	0.0000	2
	0.0625	0.3164	0.7725	4
	0.3164	0.7725	0.9845	6
	0.7578	0.8922	0.9999	12
10	0.0000	0.0000	0.0000	2
	0.0010	0.0563	0.5245	4
	0.0563	0.5245	0.9616	6
	0.4999	0.9560	0.9998	12
20	0.0000	0.0000	0.0000	2
	0.0000	0.0032	0.2751	4
	0.0032	0.2751	0.9247	6
	0.2499	0.9140	0.9996	12

[a] Prepared with the help of Dr. Gene Hertel, Proteus Corporation.

By $\mathcal{F}$ we represent the dissipation imposed upon the model in the forms of filtering and bottom friction. The filter is a Shapiro filter, as described in [22]. Such filtering can be viewed as an approximation of a partial differential operator which describes high-order lateral friction. For details, see Shapiro [23]. In our implementation, we specify the filter by order (n), the nuber of iterations per application (m), and the number of time steps (p) between successive filter operations. A Shapiro filter of order n is equivalent to a lateral friction term proportional to ∇^{2^n} with the addition of cross terms. Thus a higher order filter is more highly scale selective (i.e., has a steeper response function in wave number space) than a lower order one. The response function is tabulated in Table II. As an example, FIL(4, 1, 2) is a fourth-order filter applied once every other time step. FIL(N, 1, 1) is Shapiro's [23] ideal Nth-order low pass filter. Bottom friction is included as a linear drag; as will be seen

below, in the discrete model it appears only in the deepest level. Parameterization of bottom drag is exactly as in [22, Eq. (4)]:

$$\left(\frac{\partial}{\partial t} + \varepsilon \mathcal{J}(\psi, \cdot)\right)\zeta + \psi_x = -\kappa\zeta \qquad \text{for} \quad \zeta, \psi \text{ at the lowest level.} \tag{3}$$

Here κ is a dimensionless decay parameter.

The above parameters define the physical model. We distinguish these from the computational parameter set introduced below which determines the numerical performance of the discretized version of the model. The open lateral boundary conditions are those specified by Charney *et al.* [4], i.e., streamfunction specified everywhere on the boundary and vorticity specified at inflow points. For the case of a flat bottom and horizontally constant temperature at the top, the vertical boundary conditions are given as:

$$\psi_z\Big|_{\text{top}} = \psi_z\Big|_{\text{bottom}} = 0.$$

The general vertical boundary conditions are given as follows, in terms of the vertical velocity w at the top and bottom:

$$w_{\text{top}} = \frac{D}{Dt}\sigma\psi_z\Big|_{\text{top}}, \qquad w_{\text{bottom}} = \frac{D}{Dt}\sigma\psi_z\Big|_{\text{bottom}}.$$

Nonzero vertical velocities at top or bottom result in loss of uniformity of convergence of expansion (6), introduced in Section 2.2, of ψ and ζ in terms of flat bottom vertical modes; this complicates evaluation of component-by-component response in the collocation method, but presents no significant implementation problems in the finite difference method.

Treatment of vertical boundary forcing has been described in detail elsewhere: the methods described by Bretherton and Karweit [3] and by Flierl [6] can be adapted to our model. It is important to recognize a basic difference between the open boundary problems of interest here and the case of a closed boundary. In the closed boundary problem, the complete relationship between the streamfunction values at adjacent levels of depth cannot be given explicitly by boundary conditions; rather, it must be determined in part by the imposition of internal physical constraints such as conservation of mass across each level. However, for the open boundary problem, the streamfunction must be specified at every point on the boundary, except only for a global additive constant which has no physical or computational significance. Care is required in the specification of the streamfunction on the boundary, since the vertical differences of the streamfunction are related to the buoyancy flux, but no implicit constraints are involved. Physically, the constraint for the closed adiabatic quasigeostrophic system involves boundary temperatures (buoyancy) being set

consistently by internal advection, whereas in the open case, externally advected values are specified. In the framework of the quasigeostrophic approximation, this amounts to the implicit requirement that U_1, the first-order velocity term in Rossby number, be consistent with first-order conservation of mass.

In our computational tests, we concentrate on Rossby waves. The Rossby waves we use are solutions of (1) and (2) with $\mathcal{F} = 0$ of the form

$$\zeta = -(1 + \lambda_j^2) \sin(\mathbf{k} \cdot \mathbf{x} - \omega t)\, Z_j(z), \tag{4a}$$

$$\psi = \sin(\mathbf{k}\mathbf{x} - \omega t)\, Z_j(z) - \gamma y, \tag{4b}$$

$$\mathbf{k} = (k, l);$$

Z_j is the jth normal mode of the vertical operator in (2) with eigenvalue $-\lambda_j^2$. For any wave we wish to simulate, we can choose $k^2 + l^2 = 1$, which is equivalent to choosing the scale length d so that one wavelength is equal to 2π. With this scaling, 4a, 4b will be a solution of (1) and (2) if

$$\omega = [-k/(1 + \lambda_j^2)] + \varepsilon k \gamma. \tag{5}$$

2.2 *Discrete Model and Methods*

The basic strategy of the method used to solve (1) and (2) takes advantage of the fact that (1) contains all of the time derivatives while (2) contains all of the depth derivatives. The method currently employed uses bilinear finite elements in horizontal space and second-order Adams–Bashforth differencing in time; for details, see [8]. Given initial ψ and ζ fields, the Adams–Bashforth time discretization of Eq. (1) [8, Eq. (10b)] provides a method of calculating ζ at the next time step. Since depth appears only as a parameter in (1), this prognostic calculation can proceed level-by-level barotropically. We then compute the streamfunction ψ by solving the Poisson-type equation (2), using the new value of ζ as the right-hand side. We use the method of separation of variables to solve (2) as a sequence of uncoupled 2-D Helmholtz equations. This allows the use of available fast efficient codes [1] for the solution of such Helmholtz equations. The separation of variables process proceeds as follows: write

$$\psi = \sum_i \hat{\psi}_i(x, y, t)\, Z_i(z), \qquad \zeta = \sum_i \hat{\zeta}_i(x, y, t)\, Z_i(z), \tag{6}$$

where Z_i is the ith eigenfunction of the depth operator in 2,

$$\Gamma^2(\sigma(z)\, Z_i'(z))' = -\lambda_i^2 Z_i(z), \tag{7a}$$

$$Z_i'(0) = Z_i'(-H) = 0, \tag{7b}$$

and λ_i corresponds to the reciprocal of the ith Rossby deformation radius. We normalize the Z_i so that

$$(1/H)\int_{-H}^{0} Z_j(z)\, Z_k(z)\, dz = \delta_{jk}.$$

For a solution of this form, (2) becomes

$$\nabla^2\hat{\psi}_i - \lambda_i^2\hat{\psi}_i = \zeta_i \tag{8}$$

for integers $i \geqslant 0$.

The lateral boundary conditions must, of course, be transformed in the same fashion. New values of ψ at each level are constructed from the $\hat{\psi}_i$ to complete the time step.

As in the earlier barotropic version of the model, the lateral boundary conditions are treated by using the dynamic equations to uncouple the boundary from the interior so they can be treated as separate algebraic entities. Details of this procedure can be found in [8].

The separation of variables procedure (6)–(8) has been implemented numerically in two ways: by a finite difference method and by a collocation method. In the finite difference method, the depth operator is replaced by a difference operator. This is exactly the level method as used in process studies by other investigators, e.g., [3].

The vertical structure of the model is given in Fig. 1. The levels at which ψ and ζ are calculated are shown as dashed lines. In the finite difference model, the dimensionless stratification parameter σ is given at levels shown as solid lines. In the collocation model, stratification data enters the calculation implicitly.

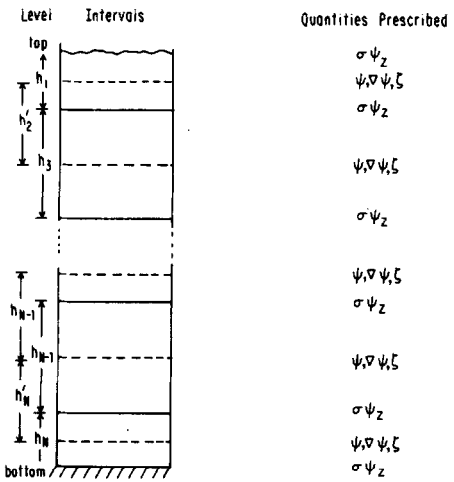

FIG. 1. Structure of depth discretization of baroclinic model.

2.2a. *The Finite Difference Model*

Let $\psi_j(x, y, t) = \psi(x, y, z_j, t)$, where z_j is the (dimensionless) vertical coordinate of the jth level. We write the finite difference operator as follows:

$$(\sigma\psi_{1z})_z \cong \frac{1}{h_1}\left\{\sigma\psi_z\Big|_{\text{top}} - \frac{\sigma}{h_2'}(\psi_1 - \psi_2)\right\}, \tag{9a}$$

$$(\sigma\Psi_{jz})_z \cong \frac{1}{h_j}\left\{\sigma_{j-1}\frac{\psi_{j-1} - \psi_j}{h_j'} - \sigma_j\frac{\psi_j - \psi_{j+1}}{h_{j+1}'}\right\}, \qquad 0 < j < N \tag{9b}$$

$$(\sigma\psi_{Nz})_z \cong \frac{1}{h_N}\left\{\sigma_{N-1}\frac{\psi_{N-1} - \psi_N}{h_N'} - \sigma\psi_z\Big|_{\text{bottom}}\right\}. \tag{9c}$$

The h_i are the level depths shown in Fig. 1.

The variables $\sigma\psi_z|_{\text{top}}$ and $\sigma\psi_z|_{\text{bottom}}$ represent temperature anomaly distributions at the top and bottom boundaries which must be determined prognostically (by advection) except in the simplest cases studied here which correspond to uniform temperature surfaces. If we let $\boldsymbol{\psi} = (\psi_1, \psi_2, \ldots, \psi_N)^{\mathrm{T}}$, we may write (9) in vector form:

$$(\sigma\psi_z)_z \cong L\boldsymbol{\psi} + \begin{pmatrix} \sigma\Psi_z|_{\text{top}} \\ 0 \\ 0 \\ \vdots \\ 0 \\ \sigma\psi_z|_{\text{bottom}} \end{pmatrix}. \tag{10}$$

The eigenvalues $-\tilde{\lambda}_i^2$ of L approximate the eigenvalues $-\lambda_i^2$, $i = 0, 1, \ldots, N-1$, of the continuous operator $(\sigma\psi_z)_z$ with boundary conditions (7b) for an N-level model. Physically, λ_i is the reciprocal of the ith internal deformation radius. Since the rows of L all sum to zero, $\tilde{\lambda}_0^2 = \lambda_0^2 = 0$ and thus the discrete system, like the continuous system, has a barotropic mode. However, for the baroclinic modes, the approximation $-\tilde{\lambda}_i^2$ to $-\lambda_i^2$ deteriorates with increasing i. For fixed i, $-\tilde{\lambda}_i^2$ converges to $-\lambda_i^2$ as the number of levels of N increases; but for any finite N, $-\tilde{\lambda}_i^2$ will be a very poor approximation of $-\lambda_i^2$ for $i \approx N$. This can be illustrated with the simple example of a model depth structure with $\sigma = \Gamma^2 = 1$, total depth $= \pi$, and equally spaced levels. In this case, the eigenvalues of both the continuous operator and the finite difference approximation are known exactly. The comparison between the exact and approximate eigenvalues is shown in Table III. As the number of levels increases, $-\tilde{\lambda}_1^2$ approaches 1, as shown in row 2 of Table III. But looking down the column corresponding to the 8-level simulation, we see the error increase from 1% for the first mode to 19% for the fourth. A 16-level example would show a marginally better value for $-\tilde{\lambda}_1^2$, and a considerably better value for $-\tilde{\lambda}_4^2$, but still the error in $-\tilde{\lambda}_{15}^2$ would be high.

TABLE III

Comparison of Eigenvalues of Depth Operator with Finite Difference Approximation for Constant Stratification Parameter

Mode	Eigenvalues of finite difference operator: Number of levels 2	4	8	Eigenvalues of continuous operator
0 (barotropic)	0	0	0	0
1	−2	−0.95	−0.99	−1
2		−3.24	−3.80	−4
3		−5.53	−8.01	−9
4			−12.97	−16

Note. Levels are equally spaced. Basin has total depth π.

TABLE IV

Computational and Model Parameters for Rossby Wave Tests with Constant Stratification

Variable	Description	Value[a]
Computational parameters		
N	Number of lateral gridpoints/basic width, including endpoints	33
ν	$\pi d(N-1)/L$ = number of gridpoints/half wavelength	9.4
Δt	Dimensionless time step	
τ	$P\beta d/(2\Delta t)$ number of time steps/half period	64–128
K	Linear, bottom drag coefficient, (scale time)$^{-1}$	0.016–0.032
Regional parameters		
d	Scale length	47.75 km
H	Total basin depth	1
f_0	Coriolis parameter, MODE region	7.05×10^{-4} sec
N	Typical buoyancy frequency, main thermocline, MODE region (see MODE Atlas)	0.005 sec^{-1}
Γ^2	$(f_0 d/N_0 H)^2$	0.0181
$1/\beta d$	Time scale	9.97×10^5 sec =11.53 days
σ	Variation of stratification with depth	1
X_B	Dimensionless width of model basin	3.5π
P	Dimensional period	
L	Dimensional basin size	525 km
L_z	Dimensional total depth	5 km

[a] Numerical values refer to the tests with constant stratification.

In the process of computing Rossby waves by the finite difference model, λ_i^2 is replaced in dispersion relation (5) by $\tilde{\lambda}_1^2$, and the frequency (and hence the phase speed) of the waves will be in error for the baroclinic modes. This phase error is readily apparent in our finite difference test calculations. Lateral and temporal discretization also gives rise to errors in the dispersion relation.

2.2b. *The Collocation Model*

In the collocation scheme the exact eigenvalues and eigenvectors $-\lambda_i^2$ and $\mathbf{Z}_i$ must be input to the model. In the case of constant σ, these are known exactly. In the general case of nontrivial dependence of σ upon z, $-\lambda_i^2$ and $\mathbf{Z}_i$ must be determined numerically by solving (7) on a fine grid. In this case, (5) is reproduced exactly, and there will be no phase error in the Rossby wave tests due to vertical discretization.

2.2c. *Computational Parameters*

A list of computational and model parameters appears in Table IV. That table contains definitions of each parameter along with relevant values for the tests shown in Table I. Horizontal and temporal resolution parameters were explored in [8]. Here we use horizontal resolution found to be adequate for Rossby waves in that study.

3. Results of Single Rossby Waves with Constant Stratification

3.1 *Choice of Wave Parameters*

In this series of experiments, single Rossby wave simulations were run in a model region 1.75 wavelengths square with stratification parameters chosen so that σ in Eq. (2) is held constant. In all of these calculations a 33×33 lateral grid was used. This corresponds to approximately 10 points/half wavelength. The scale V_0 is set implicitly by the choice of ε. The scale depth is set to the total depth, rather than the thermocline depth in these simulations. As noted in Table IV, we have chosen to relate τ, the temporal resolution of the model, in terms of the basic wave period. Since the period of a given wave depends on the mode number, the stratification, and the strength of the advection present, the actual time step Δt will vary from wave to wave for a given value of τ. In this case of constant stratification, equally spaced depth levels are the proper choice. In fact, with this choice one would expect the finite difference method to perform better than it would in a more realistic setting, since the finite difference operator with equally spaced levels is second-order accurate with constant σ; in general it is only first-order accurate.

In the case of varying stratification with depth, an argument similar to the derivation of the nodal positions for Gaussian quadrature (see, e.g., [9]) indicates that in an N-level collocation calculation the levels should be placed at the zeros of the Nth baroclinic mode. A heuristic justification for this procedure is that for this choice of levels, no aliasing error will result from the presence of the (unresolved)

Nth baroclinic mode. This formulation reduces to that of equal spacing for constant stratification, since in that case the modes are cosines.

Calculations were performed for two values of the β-Rossby number. The initial tests were performed with $\varepsilon = 0.4$ as in several of the calculations shown in [8]. Though the value is low from a physical standpoint, it is large enough so that nonlinearity is dynamically significant. A moderate Rossby number, $\varepsilon = 1.5$, was used in further tests. A very similar Rossby number ($\varepsilon = 1.48$) was used in the barotropic forecast experiments reported in [22], and is also used in the generation of the simulated baroclinic data set.

3.2 *Weakly Nonlinear* ($\varepsilon = 0.4$) *Rossby Wave Tests*

As noted in Section 2.2a, in the finite difference model, truncation error in the approximation to the depth operator gives rise to an inaccurate Rossby deformation radius. This is turn results in an error in the phase speed which in turn leads to a phase shift between the computed and analytic solutions. As the predicted field

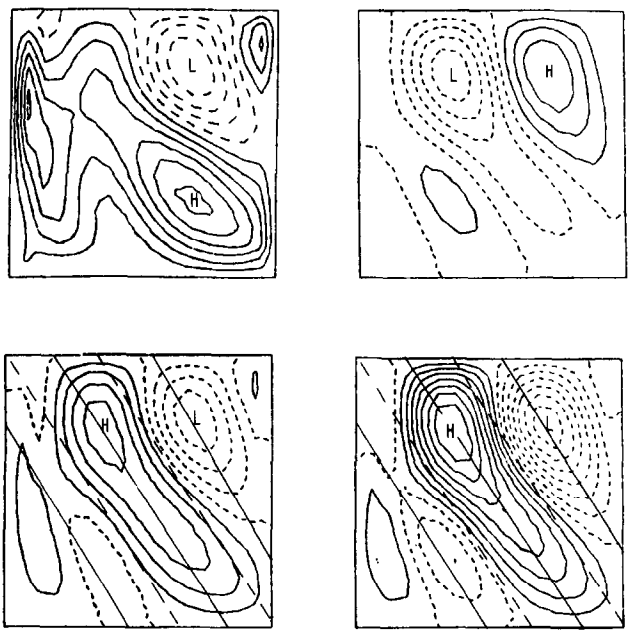

FIG. 2. Comparison of forecast streamfunction errors after one period. Clockwise from upper left: barotropic mode, maximum error = 0.013; first baroclinic mode, 2 levels, maximum error = 0.25; first baroclinic mode, 4 levels, maximum error = 0.082; first baroclinic mode, 8 levels, maximum error = 0.023. The topmost level is displayed for the baroclinic calculations. Contours of linear phase error neglecting boundary interactions superimposed upon four- and eight-level maps. Solid lines in centers of patterns are crests. Dashed lines are nodes. Other solid lines are troughs.

evolves, it interacts nonlinearly with the analytically derived wave imposed at the boundary to produce small scale motions which modify the wave field and distort the structure of the predicted field. Figure 2 shows the error fields for the barotropic mode and the top level of the first baroclinic mode simulations for three choices of vertical resolution. The error fields shown correspond to finite difference runs numbered 1–4 in Table Ii. The error due to the phase shift alone, neglecting nonlinear effects and boundary effects, can be calculated directly. Contour lines of the error due to phase shift are shown superimposed on the four- and eight-level error fields in Fig. 2. The maxima of these error fields are 0.048 and 0.012, respectively. This illustrates the second-order convergence of the finite difference method with equal spacing. The most striking feature of the phase shift error fields is the coincidence of the crests, troughs, and nodes of the phase shift error with those of the total error in the interior. In the light of this, the error fields appear to be a combination of phase shift errors and box modes arising from boundary errors in the barotropic calculations. The barotropic calculation also contributes some phase shift due to lateral and temporal truncation error. In the eight-level simulation, the maximum error is approximately the sum of the maximum errors of the barotropic error field and the phase shift error, and thus these two sources account for all of the error amplitude.

Therefore, for the waves studied here, we conclude that eight levels are required in the finite difference simulation to achieve error control comparable to that in the barotropic code, i.e., to control the error to be of the same size as that associated with our choice of horizontal resolution. In the collocation tests at $\varepsilon = 0.4$ for baroclinic modes 1–3, error control is comparable to that in the barotropic mode. The collocation runs numbered 2 and 3 show little difference in error between two- and four-level simulations. The two-level simulation has only a barotropic and first baroclinic mode.

Although there are regions of the ocean where the energy of the flow is concentrated in the barotropic and first baroclinic modes, these are known to be phenomena of interest that occur on finer vertical scales. In the MODE eddies, energy was concentrated in the barotropic and first baroclinic modes, but there were instances of higher modes in the data. In the POLYMODE data there are samples of high internal mode energies. Additionally, the ocean may transfer energy to higher vertical modes and dissipate it. In that case, forecasting requirements may dictate that the model reproduce this process. Finally, from a strictly computational viewpoint, we believe higher resolution of nonlinear flows may be necessary in order to represent multiple nonlinear interaction correctly.

In the analytic case of Rossby waves without advection, the nonlinear term of (1) vanishes identically and the nonlinear term in the numerical calculation consists exclusively of interaction between the calculated field and the analytic solution imposed at the boundary. When advection is imposed upon the wave field, the interaction between the wave field and the mean flow gives rise to a nontrivial nonlinear term from the beginning of the simulation. The fact that the form of the nonlinear interaction between the mean flow and the wave field is known explicitly

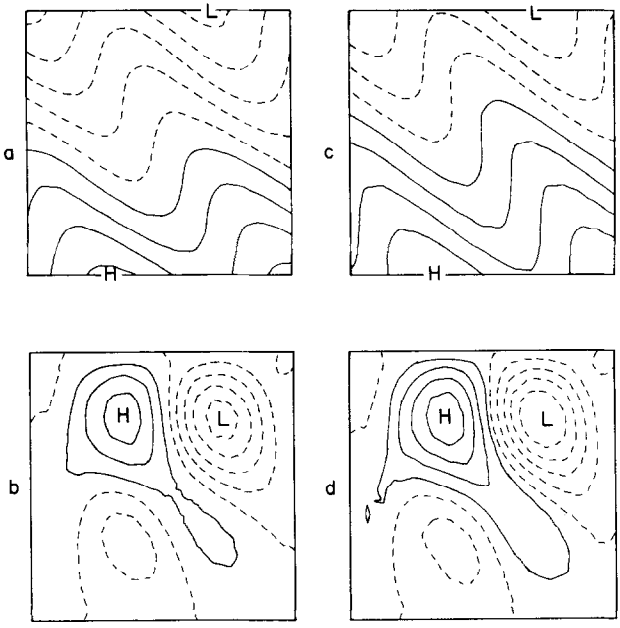

FIG. 3. Rossby waves with advection. Streamfunction fields and their associated error fields. Wave field similar to that shown in Fig. 1 but with mean eastward advection = 0.5 added (run 7 in Table Ii). Streamfunction amplitude normalized to one. Parts a, b: top level of two-level simulation; streamfunction and error field, respectively; maximum absolute error = 0.31. Parts c, d: top level of four-level simulation; maximum absolute error = 0.10. Normalized RMS error = 0.034.

means that an advected Rossby wave simulation can be designed in which the nonlinearity has any desired strength. We will exploit this in Section 4.

The simulations in which we impose advection on the Rossby wave field are thus a step closer to nonlinear reality. Figures 3 and 4 illustrate the results of a finite difference test in which the wave shown in Fig. 2 is subject to a eastward advection speed = 0.5 in the scale of the problem ($\approx$2 cm/sec). Two- and four-level simulations are compared. After a full period, 11.69 of scale time, these simulations show the characteristic Rossby wave pattern. Referring to Table IV, this corresponds to 135 days in dimensional time. The error fields reflect the structure of a phase error, with some box mode structure appearing from the difference in phase between the driving (boundary) field and the interior wave field. The vorticity error fields, as one might expect, show finer structure. The appearance of finer structure in the vorticity error of the four-level simulation (Fig. 4d) reflects the fact that fine structures may represent a larger portion of the error field shown in Fig. 4d, even though they may be of smaller absolute amplitude. Care should be taken in the interpretation of maps such as these with differing contour intervals.

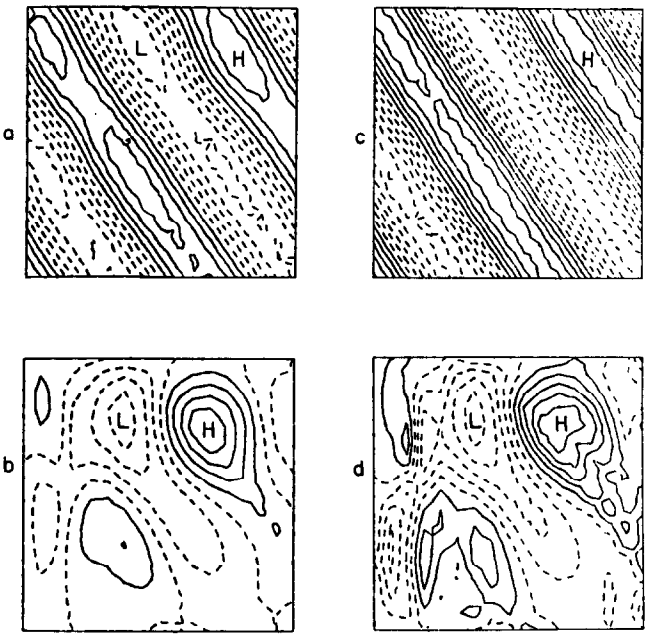

FIG. 4. Rossby waves with advection. Vorticity fields and their associated error fields. Same experiment as Fig. 3. Parts a, b: top level of two-level simulation; vorticity and error field respectively; maximum absolute error = 0.35. Parts c, d: top level of four-level simulation; vorticity and error field, respectively; maximum absolute error = 0.12.

The analogous simulation by the collocation method is so accurate (0.3% ψ, 2.6% ζ after two periods) that the plots are not of great interest. In these cases, i.e., Rossby waves at low Rossby number with and without advection, the collocation method is considerably more efficient. Since the difference in actual computation between the finite difference and collocation methods lies entirely in the representation of the eigenvalues and eigenvectors of the depth operator, the two methods require the same amount of computer time per time step. These tests alone, however, are not sufficient to rule out the finite difference method generally on the grounds of computational inefficiency despite their comparative disadvantage here. Rossby waves are an exact solution to the algebraic equations that determine the computational collocation method, and thus the collocation method is expected to perform better in these tests. Since the error can be controlled at the 10% level in a finite difference calculation of this length, the finite difference method remains a practical tool. Its performance relative to the collocation may improve in other situations and it also has the important advantage of more straightforward implementation for the cases of nonconstant surface temperatures and nonhorizontal boundaries.

In the simulations shown in Figs. 2–4, there is no dissipation, and noise arising

from computational errors, including near gridscale features, is permitted to accumulate. For this reason, dissipation free computations do not in general remain well behaved over integrations several periods in duration. The problem becomes more severe in high baroclinic mode finite difference calculations. If the model is driven from the boundary with the analytic solution for a high baroclinic mode Rossby wave, truncation error in the vertical grid will produce a phase error in the interior, as noted in Section 2. The phase difference between the interior field and the boundary data produces by nonlinear interaction a rapid accumulation of small scale features near the boundary.

As in [22], we chose to impose dissipation in the form of a scale selective filter. Details of the use of this method on the barotropic version of the forecast model may be found in [22]. The fourth-order filter that had been successful with the barotropic model provided insufficient dissipation for the third mode finite difference test run with our chosen parameters. It is clear from Eq. (9) that higher baroclinic mode waves have lower frequencies. Therefore, if the number of time steps per period is held constant, the time step will increase. In the case of the four-level third baroclinic mode finite difference simulation, the calculation could not be stabilized with a time resolution $\tau = 64$. With temporal resolution of $\tau = 128$ and a second-order Shapiro filter applied every time step, the third baroclinic mode four-level simulation ran stably for two periods, albeit with large errors. The third mode has a considerably lower frequency than the barotropic and first baroclinic mode, and thus $\tau = 64$ implies a longer time step (Δt) for this run than for runs 1–11. Spurious barotropic and low baroclinic mode disturbances are thus poorly resolved. The fact that run number 12FD with $\tau = 128$ ran successfully, while a similar run with $\tau = 64$ became unstable very quickly is evidence that the latter run failed due to violation of a CFL condition. This was not uncommon in our experience with the model.

Accurate reproduction of second and third baroclinic modes is not possible with a four-level finite difference simulation, as runs 9 and 12 demonstrate. However, with appropriate filtering and time resolution, finite difference calculations can proceed without catastrophic instability caused by high baroclinic mode disturbances. Vertical filtering (or equivalently damping higher modes) offers some hope for further stabilization of such calculations. This was not used in the present series of tests. To interpret the horizontal filtering, note that [23] a Shapiro filter of order n is, except for cross terms, equivalent to a ∇^{2^n} operation.

3.3 *Moderately Nonlinear* ($\varepsilon = 1.5$) *Rossby Wave Tests with Constant Stratification*

In the next series of tests, ε was set to 1.5. The advected wave tests were run with mean flow = 0.2. Only the first baroclinic mode was simulated. Lateral dissipation in the form of a second-order Shapiro filter was imposed at varying time intervals. In some of the runs, bottom friction was imposed with coefficients 0.016 or 0.032. These values correspond to spin-down times of 62.5 and 31.25, respectively. The dimen-

sionless wave period in these simulations is 13.8 in the calculations with advection and 8.9 in the calculations without advection. All other computational parameters were held constant. Since ε and γ influence the period of the advected waves, the actual time steps differed from the lower Rossby number simulations because of our adopted convention of fixing the time resolution in terms of the wave period. In this series of tests (runs 13–17) τ, the number of time steps/half period, was fixed at 64.

In the tests of the finite difference method for $\varepsilon = 1.5$, the errors, as expected, were somewhat larger than they were in the low Rossby number case, but could still be controlled near 10% for two periods. The first baroclinic mode simulation without advection (run 13 in Table Ii) ran to completion with no filtering or bottom friction and RMS streamfunction errors between 9.5% and 16% (for the third and first levels, respectively) after two full periods. It was clear from this run that dissipation-free calculation could not proceed much further in this case. During the time interval from $1\frac{3}{4}$ to 2 periods, the maximum velocity in the top layer went from 1.0, which is normal, to 4.3, while the energy approximately doubled. Computation of a flow with this high velocity will be subject to a stricter CFL condition than the original flow.

We note here that in this run energy fluxes from the boundary may occur due to the disparity between the analytic and numerical solutions. We anticipate the simulation of real flows in which energetic structures enter the computational domain through the boundaries, causing rapid increase in the total energy of the field. In either of these cases, the generalization that more energetic flows are subject to more stringent stability conditions holds.

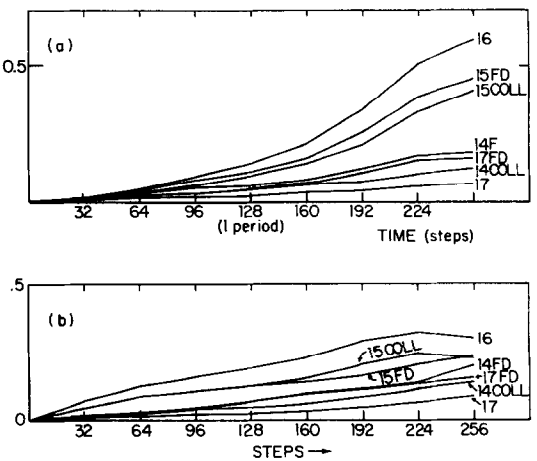

FIG. 5. RMS streamfunction error vs. time. Value normalized by RMS of exact field; $\varepsilon = 1.5$, advection = 0.2, angle of propagation = 0.5932 radians from due east. Part a: top level of four-level simulation. Part b: bottom level of four-level simulation.

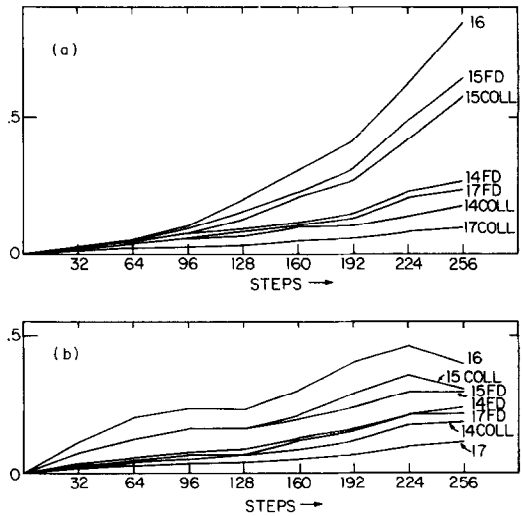

FIG. 6. RMS vorticity error vs. time. Values normalized by RMS of exact field. Parameters as in Fig. 5. Part a: top level of four-level simulation. Part b: bottom level of four-level simulation.

Violation of such a condition is probably the immediate cause of failure in most such situations, as in the failure of a run similar to 12 with $\tau = 64$, noted in the preceding section. The summarized results of our tests of advected Rossby waves with Rossby number 1.5 are shown in Table Ii, examples 14–17, and Figs. 5–9.

Figures 5 and 6 show the evolution of RMS streamfunction errors and vorticity errors as functions of time at the top and bottom levels. The errors are consistently higher in the top level than in the bottom level for runs 15 (finite difference) and 16 (collocation). These were the runs with bottom friction in which one expects increased errors because the parameters of the wave imposed at the boundary represent a dissipation-free solution to (1) and (2). Without bottom friction, there is little difference between top and bottom, as one would expect in a constant stratification run. Runs 17, the runs with the least dissipation, were the best performers in the finite difference and collocation cases. The improvement in performance was more marked in the collocation than in the finite difference case; in fact, at the third level, run 14FD finished with a slightly lower RMS vorticity than run 17FD. The energy errors (Fig. 7) exhibit a similar pattern. As expected, the runs with bottom friction show greater energy errors at the bottom level than at the top, while there is less difference in the runs without friction. The collocation runs show consistently less energy than the finite difference runs. Finite difference runs 14 and 17 are the only runs to show a positive energy error.

Since the runs in this series with the least filtering are the most accurate, one is tempted to try still weaker filtering. Some filtering, however, is necessary. With no

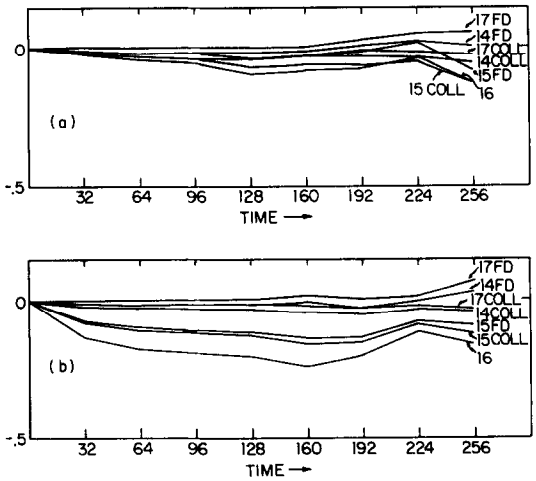

FIG. 7. Normalized RMS energy error vs. time. Part a: top level of four-level simulation. Part b: bottom level of four-level simulation.

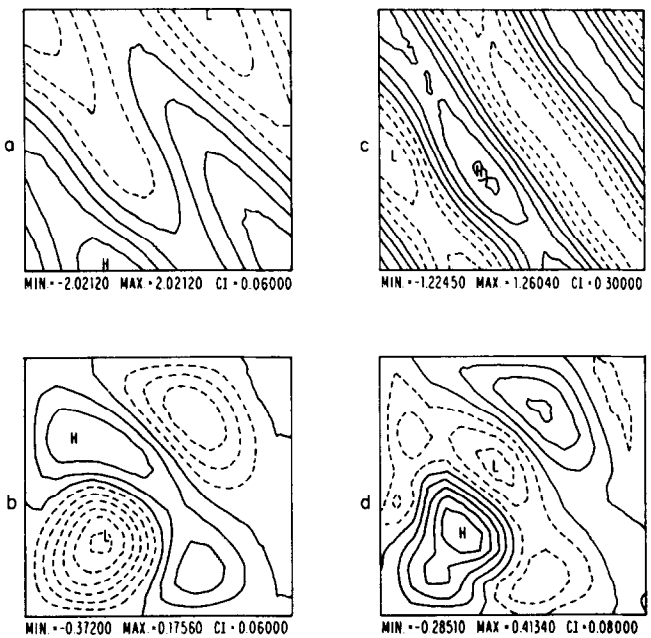

FIG. 8. Nonlinear Rossby wave fields for level 1 of run 14 (collocation) following 2 periods. Clockwise from upper left: streamfunction, vorticity, vorticity error, streamfunction error.

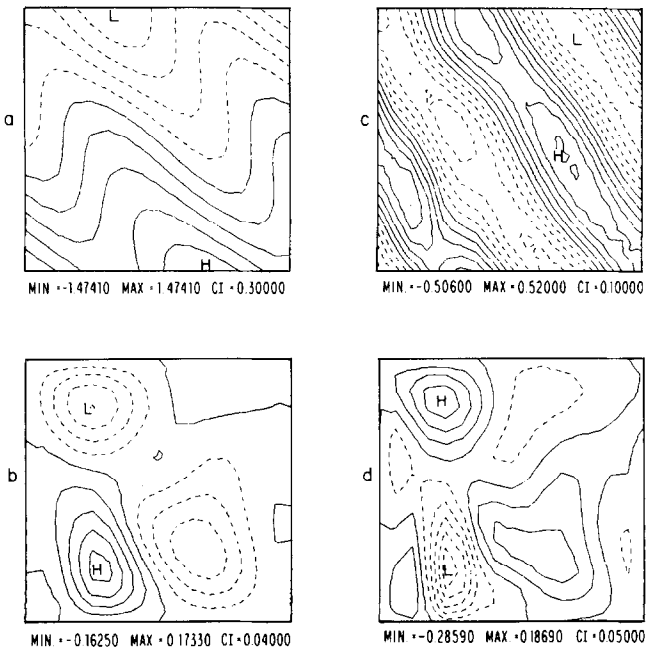

FIG. 9. Nonlinear Rossby wave fields for level 3 of run 14 (collocation), following 2 periods. Clockwise from upper left: streamfunction, vorticity, vorticity error, streamfunction error.

filter or bottom friction and other parameters as in 14–17, the collocation calculation becomes unstable in less than one half period.

Figures 8 and 9 show streamfunctions, vorticity, and associated error fields for collocation run 14 at the first and third levels after two periods. The streamfunction fields show the correct structure, while the vorticity fields have taken on a distinct waviness. The errors appear to be dominated by box modes, indicating the dominance of boundary effects in the error field. Some phase shift error is also apparent at the top level.

The third level vorticity error is concentrated in the low in the lower left quadrant and in the high in the upper left quadrant. That intense low (error extremes are -0.3 and 0.2; field amplitude $= 0.5$, both positive and negative directions; normalized RMS error at this level $= 0.23$) corresponds to the waviness of the field in the lower left quadrant. Streamfunction errors are more uniformly distributed at both levels, as one would expect.

On the basis of these results, we choose the collocation method for our tests of the model with realistic stratification. These are presented in the next section.

4. Advected Rossby Waves in a Realistically Stratified Environment

As a further evaluation of the capability of our model to deal with nonlinear problems in realistic parameter ranges, we present a series of advected baroclinic Rossby wave calculations in a realistically stratified environment. Stratification data were taken from [19].

Baroclinic modes were calculated by solving (4) numerically on a 36-point mesh. The barotropic and first three baroclinic modes are shown in Fig. 10. Several combinations of level depths were used in our tests. Most of the tests were run with levels set at 100, 400, 700, and 1400 meters. These are the depths at which data is available from USSR POLYMODE current meter array [20] which provided the first real ocean baroclinic data set to be used with this model. Optimal choices of levels (see Section 3a for definition of "optimal") were also used for four- and six-level calculations. Second-order Shapiro filtering was imposed at an interval of either one day or one half day.

The parameters in these simulations were chosen to mimic wave/wave and wave/mean flow interactions as faithfully as possible within the capabilities of this simple analytical example. The first baroclinic mode waves were chosen in each case. In the case of a Rossby wave with zonal wave number k, in a regime with β-Rossby number ε in the presence of a zonal mean flow with amplitude γ, the nonlinear term in the equation has magnitude $\varepsilon k\gamma$. With the propagation vector at an angle of 0.5932 radians (0 = due East; this was the heading of the dominant baroclinic wave in the MODE fit [13]), ε and γ are chosen to reflect different parameter ranges found in the field; a slower or larger scale wave interaction was modeled as a zonal flow advection. The results of these tests are summarized in Table Iii, runs 18–28.

These calculations were intended to run for sixty days of model time. Stable runs of that duration could not be made for two of the wave parameter choices with a time step of one day, which was the time step for the barotropic simulated data set. The case of $\varepsilon = 1.5$ and $\gamma = 4$ became unstable after 20 days of model time with time step set at a half day. It is clear in this case that the time resolution is very coarse, at

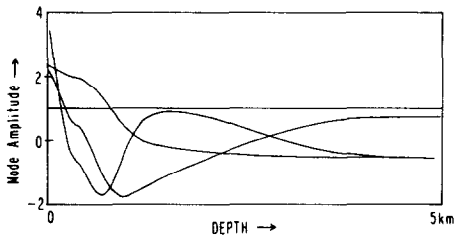

FIG. 10. Barotropic and first three baroclinic modes of depth operator with realistic stratification. Functions normalized so the mean square amplitude over the total depth is one.

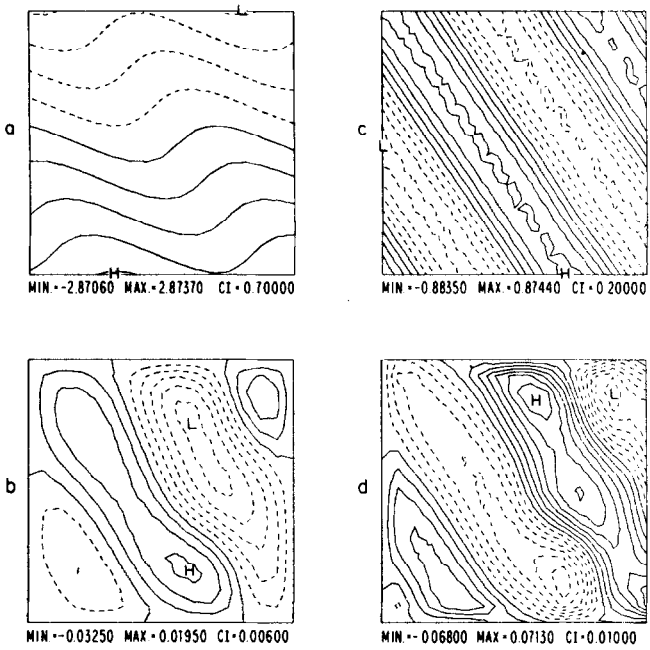

FIG. 11. Nonlinear Rossby wave fields for level 1 of run 23 after 60 days of model time. Clockwise from upper left: streamfunction, vorticity, vorticity error, streamfunction error.

$\tau = 15.7$. Run number 28 differs from run number 27 only in time resolution. The filter frequency in run 28 was two, so the time interval between successive filtrations remains the same in the two runs.

Figure 11 shows contour plots of streamfunction and vorticity and their associated errors for run number 23 after 60 days of model time. These plots show a typical well-behaved calculation. Both the streamfunction and vorticity fields have their structure intact, with no identifiable spurious features. The ranges of streamfunction and vorticity are essentially identical to the initial ones. The error fields are very smooth. The maximum streamfunction error is 0.03, or approximately 1% of the amplitude of the field including the mean flow, and 3% of the amplitude of the wave disturbance alone. The maximum vorticity error is less than 10% of the vorticity field maximum.

Figure 12 shows the streamfunction, vorticity, and associated error fields at the 700 meter level of run number 25 after 60 days of model time. The basic wave structure appears intact except for a slight irregularity in the vorticity field in the lower left corner at the error maximum. This vorticity error maximum is a rather strong one, with amplitude 0.08, compared to the predicted field maximum of 0.51. The RMS vorticity error (normalized by the RMS field amplitude) is 0.052, less than

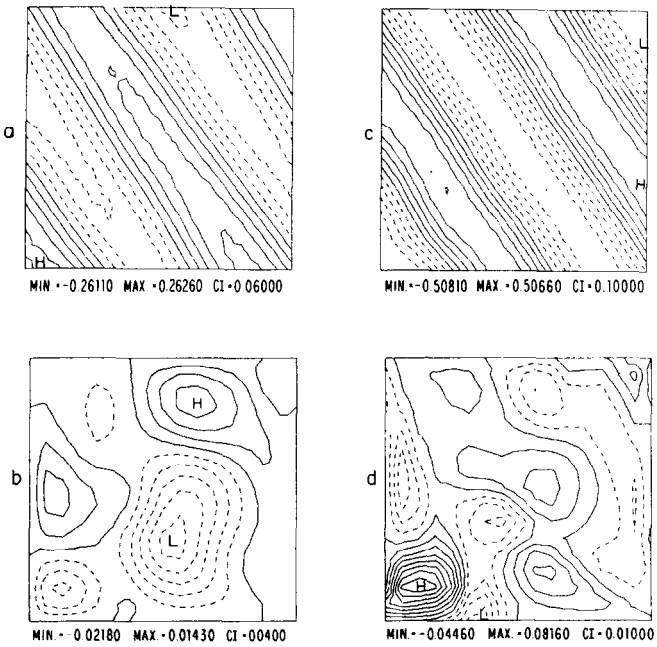

FIG. 12. Nonlinear Rossby wave fields for level 3 of run 25 after 60 days of model time. Clockwise from upper left: streamfunction, vorticity, vorticity error, streamfunction error.

a third of the ratio of the peak error to the peak field amplitude. This reflects the overall nonuniformity of the error field, i.e., the concentration of error near the maximum. The peak in the vorticity error distribution may be related to the fact that there are two boundary points near the lower left corner where the flow is tangent to the boundary.

Bennett and Kloeden [2] have suggested that the problem specified by Eqs. (1) and (2) with open boundary conditions and no dissipation may be ill posed in the classical sense because of ambiguities arising at points where the flow is tangent to the boundary. The original calculation in [4] which uses this boundary condition was done on a nonsimply-connected domain, in which such points need not arise. In our experience with this model we have encountered many instances in which the error field was dominated by structures occurring near such points. There are, on the other hand, instances where no apparent trouble arises near these points. In that same Fig. 12, there is a tangent point at the top edge near the upper left corner that is not associated with any obvious irregularity in the field. In this calculation, the temporal resolution of the wave field is so fine that the calculation will run stably for 60 days with time steps of one day. The errors are controlled at the levels shown in Table Iii by filtering with the parameters shown.

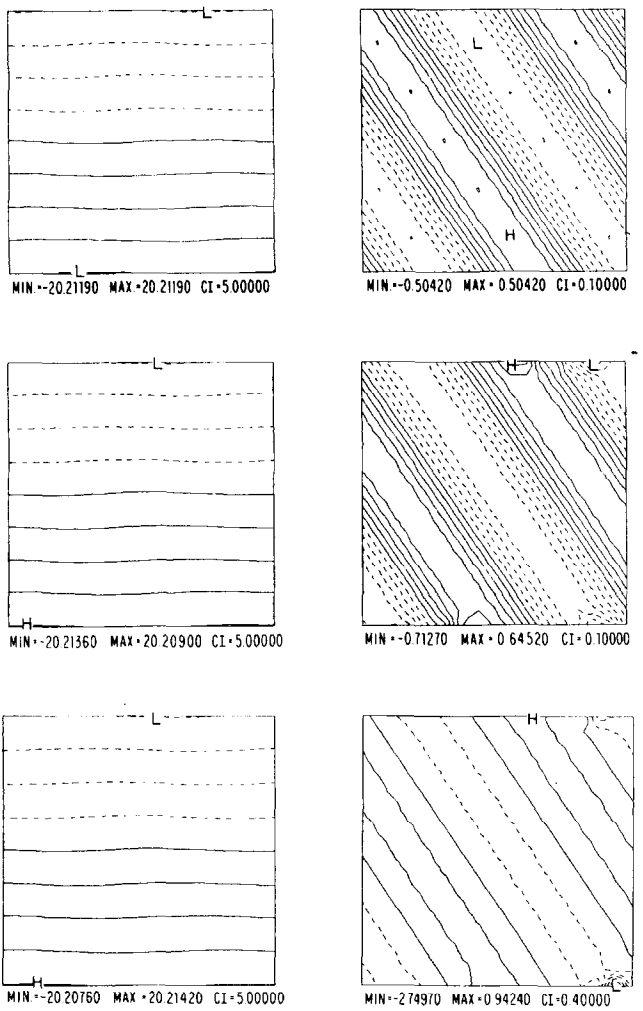

FIG. 13. Evolution of streamfunction (left) and vorticity (right) fields at 700 m from run 28 (see Table I). Top to bottom: initial field; 12 days; 60 days.

Figure 13 shows the evolution of the streamfunction and vorticity fields for run number 28 from the initial distribution to 60 days of model time at the 700 meter level. Figure 14 shows the associated error fields at 12 and 60 days. Throughout the simulation, the streamfunction field is dominated by advection. This accounts for the extremely small streamfunction errors, since the error statistics are normalized by the RMS amplitude of the streamfunction field. At 12 days, however, the vorticity field is significantly modified by concentrations of vorticity forming at the edges. The

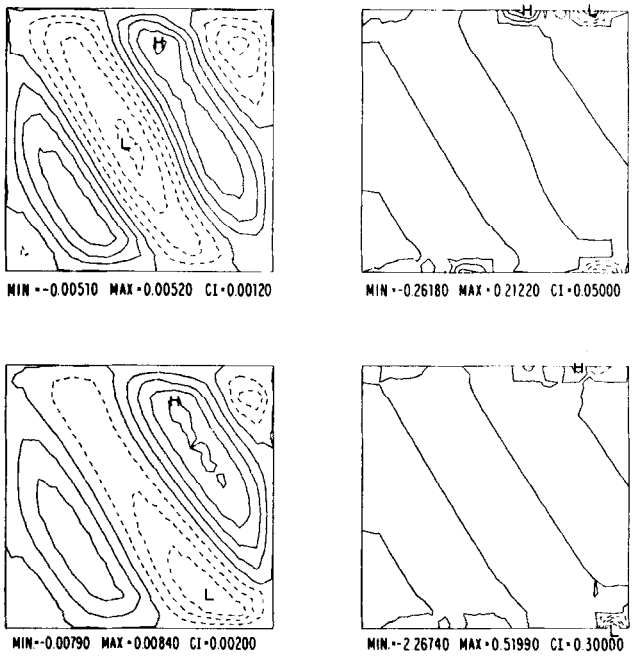

FIG. 14. Error maps of streamfunction and vorticity fields at 700 m from run 28. Top: 12 days; bottom: 60 days.

concentration of contours near eddy maxima indicates that the error field is uniform and relatively small in the interior, considering the contour interval of 0.05. At 60 days (5.19 scale time units) the vorticity field appears to be dominated by the error vortex at the lower right corner, but the interior field is relatively undisturbed.

The change in appearance of the vorticity field from 12 to 60 days is due to the contouring. Because the same number of contour intervals is used in all of Figs. 13 and 14, the contour intervals are greater in the 60-day field than in the initial and 12-day fields. The interior of the 60-day field is thus similar to the interior of the initial field, but not so well resolved by this choice of contour levels. The major features in the 60-day fields are structures which form near the boundary. The location of these structures is consistent with the hypothesis [2] that difficulties arise near points where flow is tangent to the boundary. As in the case of run 25 discussed above, [2] does not account completely for the phenomena encountered here. In particular, the occurrence of local error maxima near some of these tangent points but not near others remains unexplained.

Runs 19–22 show the characteristics of changing vertical resolution. The "optimal" levels referred to above are optimal in the sense of being the best points at which to sample a distribution containing many modes. In this case, where the profile

contains only one mode, and a rather well-resolved one at that, one does not expect a great deal of improvement. In fact, the four-level optimal spacing (run 20) does not represent a drastic improvement over run 19, from which it differs only in vertical spacing. The only significant improvement is in the maximum vorticity error. Run 21, the analogous six-level simulation, shows no improvement over run 20. Run 22 is the best run with these field parameters, differing only in frequency of filtering from run 21. Our experience with the constant stratification case is thus repeated: the run with the least filtering consistent with stability will be the run with the least error.

The large difference between minimum and maximum level-by-level RMS streamfunction and vorticity errors in this and several other runs may be a feature of the normalization. If the basic field is dominated by the first baroclinic mode, then it will be weakest at level 4 of a simulation with levels at 100, 400, 700, and 1400 meters. Since these errors are normalized by the RMS field amplitude at each level, the normalization factor is smallest where the vorticity is weakest, and therefore a barotropic disturbance in the vorticity field would appear largest at the 1400 meter level.

5. A Prototype Baroclinic Simulation Calculation

The results in [22] were intended as a preliminary study for the construction and evaluation of a baroclinic forecast model (see the conclusion section of that work). We present in this section a preliminary baroclinic calculation to show the feasibility of such a baroclinic simulated data study. As in [22], we adopt an "embedding" strategy in which an exterior numerical calculation is performed in a double-sized computational domain ($65 \times 65 \times 6$; 1000 km square by 5 km deep) to provide initial boundary and verification data for a forecast calculation over a smaller interior region ($33 \times 33 \times 6$ gridpoints; 500 km square by 5 km deep). Initial and boundary conditions for the exterior calculation were provided by the four Rossby waves found in [13] to be the best fit to the MODE data. Two of these four waves were barotropic, and the other two were first baroclinic mode waves. Only the two barotropic waves were used in the creation of the barotropic simulated data set. Stratification information was taken from [15] which is essentially identical to that given in [19]. Levels were chosen empirically by testing the capacity of various choices of levels to reconstruct several trial waveforms containing more than four modes. Time steps were set so that the highest frequency wave was resolved with $\tau = 256$. This is much finer than the temporal resolution used in the experiments described in [22]. The wave used for temporal normalization is the same as that used in [22] since the highest frequency MODE wave is barotropic. Other parameters are given in Table Iii, run 20. This choice of time resolution corresponds to a time step of approximately six hours.

Figure 15 shows the streamfunction and vorticity fields and their respective

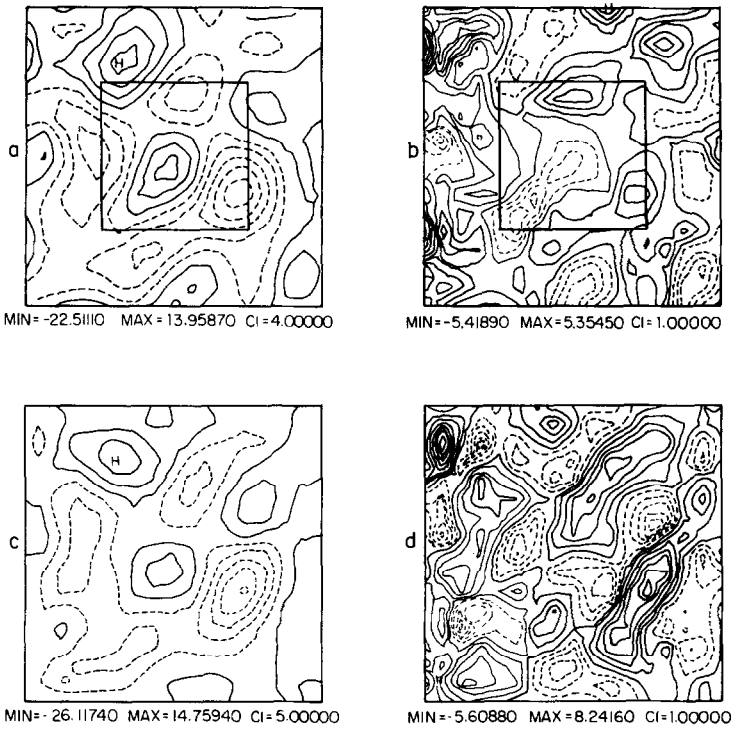

FIG. 15. Generation of baroclinic simulated data set by nonlinear evolution from initial condition of best-fit Rossby wave field to the MODE-I data. Parts a, b: streamfunction and vorticity, respectively, at 750 meters after approximately 2 years. Parts c, d: deviation from linearity of above fields, respectively. Field is 1000 km square. Boxes drawn in parts a and b represent interior domains for forecasts shown in Fig. 16. Level = 3.

deviations from the linear driving fields for the exterior calculation at the 1600 meter level after 5.5 periods of model time. At this point the simulation has reached statistical equilibrium, and the eddy structure characteristic of the nonlinear simulation is well developed (see [22, Fig. 4]). The prototype forecast experiment began at day 640 and ended at day 704. Some of the results of that experiment are shown in Fig. 16. The "exact streamfunction" comes from the exterior calculation; it is precisely an enlargement of the inner box in the upper left corner of Fig. 15. The forecast and verification fields are indistinguishable by eye. The error map, as expected, shows the errors concentrated near the boundary. The normalized RMS streamfunction and vorticity errors are 7% and 15% at this level at this time. This calculation corresponds to a benchmark calculation [22]. In that calculation, after 64 days the error was approximately 1.1%. The difference stems from the inclusion of baroclinic processes in the model. In this calculation, we can see the ability of this model to function in a realistic environment.

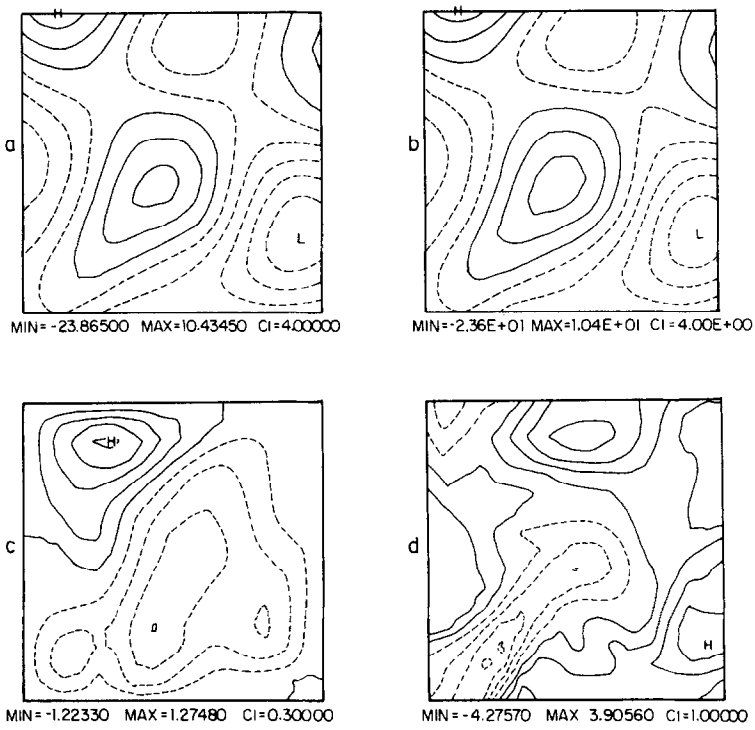

FIG. 16. Interior forecast field using interior 500 km square of simulation as initial boundary and verification data. Interior prediction begins approximately a year and 10 months into the simulation. Figure shown corresponds to the inner box in Fig. 15 approximately 2 years from the beginning of the exterior simulation. Level 3 is at 750 meters; the RMS error is 7% in streamfunction. a: forecast streamfunction. b: exact streamfunction. c: error in forecast streamfunction. d: forecast vorticity held.

6. SUMMARY AND CONCLUSIONS

The purpose of this paper is to present and document our baroclinic quasigeostrophic open ocean model and to calibrate its accuracy and stability characteristics. The test results presented demonstrate the possibility of doing such baroclinic open ocean calculations, their efficiency, and the feasibility of scientific use of models. The results depend on the qualitative character of the flow fields; for each problem type, tests were carried out over ranges of physical and computational parameters. Real quasiturbulent mid-ocean mesoscale flows of interest were aproached via a preliminary study of a set of idealized problems for which the choice of parameter ranges was guided by the nonlinear flows of ultimate concern. Our general approach was guided by our experience with the barotropic model.

We began by choosing the horizontal resolution to be used with a given problem type which, once chosen, fixes an accuracy upper limit. We then considered temporal

resolution, which can run from the (relatively inaccurate) stability limit dictated by the CFL condition to matched accuracy with the horizontal resolution and beyond (which is inefficient). Instances were encountered in which the error field was dominated by a localized feature whose growth could be controlled by increasing temporal resolution. Next the accuracy as a function of vertical resolution was carefully explored. Baroclinic effects give rise to new kinds of errors, including, of course, some which have scales and structure different from the physical fields themselves. The evaluation of model performance as a function of vertical resolution included the use of two vertical models, each of which was to some extent calibrated and intercompared.

The detailed and complete listing of results is in Tables Ii and Iii, and the discussion of results is found in paragraphs 5, 8, and 14 of Section 3 and paragraphs 5, 7, 9, and 10 of Section 4. The prototype simulation is discussed in Section 5.

We began with studies of Rossby waves, first for the case of constant stratification (typical of the main thermocline). Weakly nonlinear examples were run first. The first set of problems was run with a small Rossby number ($\varepsilon = 0.4$). For Rossby waves with no advection, ε measures the nonlinear interactions of the error field; with advection parameter γ, $\varepsilon\gamma$ also measures the magnitude of the linearized advection. Care must be exercised in the interpretation of ε in the baroclinic case, as amplitudes (and therefore effective Rossby numbers) vary with depth.

We found that for a horizontal resolution of 10 intervals per half wavelength and a time resolution of 32 intervals per half period, our finite difference method required eight levels (per half wavelength) to achieve accuracy comparable to the barotropic mode ($\sim 1\%$ period). This was the first baroclinic mode with and without advection. A two-mode collocation run achieved the same accuracy with run time equal to that for a two-level finite difference run. With four levels, the finite difference model required time resolution of 128 steps per half period and second-order Shapiro filtering every step to complete a run of two full periods of the third baroclinic mode. The accuracy of this run was poor; the object was to show that the finite difference model could make such a computation in a stable fashion. A collocation model with four modes performed the same calculation accurately with half the temporal resolution and no filtering. Reasons for this are discussed in detail in Section 2.2b; essentially, the relative efficiency and low vertical resolution required by the collocation scheme for fixed accuracy is attributable to the fact that the Rossby modes are identically the collocation modes; for more general problems, the relative accuracy is moot.

The next series of tests was also run with constant stratification, but with moderate ($\varepsilon = 1.5$) Rossby number. Care is required in the interpretation of ε as a parameter characterizing the nonlinearity of a baroclinic run because of the variation of amplitudes with depth associated with the baroclinicity. In those runs, with advection ($\gamma = 0.2$), the error could be controlled by suitable choice of filtering at the 10% level for a two-period calculation with the collocation method (4 modes) and at the 15% level with the finite difference method (4 levels); the corresponding errors respectively at $\varepsilon = 0.4$ were 1% and 8%.

The next series of Rossby wave tests was performed with realistic stratification. The collocation method was used because of its superior performance in the previous series. Three different flow regimes were chosen, each of which was designed to emulate some instance of wave/wave or wave/mean flow interaction observed in the real ocean. The three choices can be interpreted as (i) wave propagation with weak advection and a strong measure of nonlinearity ($\varepsilon = 6$, $\gamma = 0.01$); (ii) an advected wave with nonlinearity ($\varepsilon = 4$, $\gamma = 0.5$); and (iii) a strong current dominating the flow field in the presence of moderate nonlinearity ($\varepsilon = 1.5$, $\gamma = 4$).

For case (i), the streamfunction error was 23% after 60 days of model time with half-day time steps, a very fine temporal resolution of 239 steps per half period. In the other extreme case (iii) of a field dominated by advection, the strong Doppler shift necessitates a quarter-day time step for a time resolution of 31 steps per half period of the shifted wave. This result implies that in the nonlinear quasiturbulent fields of real interest, the advection by larger scale components of smaller scale ones will be the limiting factor for the choice of temporal resolution. Our simulations appear to bear this out.

In the intermediate case (ii), error control at the 1% level in streamfunction and 5% in vorticity after 60 days is achieved with half-day time steps and four levels. These results are not highly sensitive to choice of vertical collocation depths.

Finally, a preliminary calculation in an oceanically realistic quasiturbulent regime is presented using embedding, the strategy developed in the barotropic experiments. This prototype regional forecast calculation runs for 60 days with 7% streamfunction error at the end, demonstrating the ability of the model to run accurately and efficiently in such a flow regime.

During our tests, some evidence was observed for error growth of the type which might be interpreted by Bennett and Kloeden's [2] proposed mechanism at points of tangential boundary flow. However, in most instances of tangential boundary flow, no localized error growth was observed. In those cases where it did appear, it could be reduced and controlled by adjustment of the computational and filter parameters.

The finite difference model is easy to implement and offers straightforward implementation of vertical forcing. It has not, however, performed as accurately or efficiently as the collocation method in this series of tests.

The collocation method performed consistently more accurately and efficiently than the finite difference method. Choice of vertical levels and evaluation of performance as a function of vertical resolution is less straightforward, as is implementation of vertical forcing.

The baroclinic model has now been tested and validated in the parameter range appropriate for studies on mesoscale ocean data. Preliminary calculations indicate the feasibility of using the model for forecast studies. Such forecast studies using real and simulated data now form a major part of the authors' current research effort. Other laboratories currently use this model in a variety of military and civilian applications. The quantitative results presented here are intended as background for critical analysis of results obtained from the model.

ACKNOWLEDGMENTS

This research was supported by a contract from the Office of Naval Research (N00014-75-C-0225) and a grant from the National Aeronautics and Space Administration (NASA-NSG-5228) to Harvard University. The computations were performed at the Goddard Laboratory of Atmospheric Sciences (NASA-GSFC); we are grateful for the use of this facility and for the help of the support staff. It is a pleasure to thank our programmers Messrs. Jonathan Groisser and Wayne Leslie for their valued assistance. This is MODE contribution No. 178 (POLYMODE).

REFERENCES

1. J. C. ADAMS, A. C. CLINE, M. A. DRAKE, AND R. A. SWEET, Eds., "NCAR Technical Note NCAR-TN/iA-105," NCAR Software Support Library, Vol. 2, National Center for Atmospheric Research, Boulder, Colorado, 1975.
2. A. F. BENNETT AND P. E. KLOEDEN, *J. Atmos. Sci.* **35** (1978), 990.
3. F. B. BRETHERTON AND M. J. KARWEIT, *in* "Numerical Methods of Ocean Circulation," Ocean Affairs Board, National Research Council, Washington, D.C., 1975, 237.
4. J. G. CHARNEY, R. FJORTOFT, AND J. VON NEUMANN, *Tellus* **2** (1950), 237.
5. G. R. FLIERL, *Dyn. Atmos. Oceans* **1** (1977), 443.
6. G. R. FLIERL, *Dyn. Atmos. Oceans* **2** (1978), 341.
7. D. B. HAIDVOGEL, *in* "Eddies in Marine Science" (A. R. Robinson, Ed.), Springer-Verlag, New York, 1982.
8. D. B. HAIDVOGEL, A. R. ROBINSON, AND E. E. SCHULMAN, *J. Comput. Phys.* **34** (1980), 1.
9. E. ISAACSON AND H. B. KELLER, "Analysis of Numerical Methods," Wiley, New York, 1966.
10. M. G. MARIETTA AND A. R. ROBINSON, "Proceedings of a Workshop on Physical Oceanography Related to the Subseabed Disposal of High Level Nuclear Waste," SAND 80-1776, Sandia National Laboratories, Albuquerque, N.M., 1980.
11. J. C. MCWILLIAMS, *J. Phys. Oceanogr.* **6** (1976), 810.
12. J. C. MCWILLIAMS, *Dyn. Atmos. Oceans* **1** (1977), 427.
13. J. C. MCWILLIAMS AND G. R. FLIERL, *Deep-Sea Res.* **23** (1976), 285.
14. THE MODE GROUP, *Deep-Sea Res.* **25** (1978), 859.
15. THE MODE-1 ATLAS GROUP, "Atlas of the Mid-Ocean Dynamics Experiment (MODE-1)," MIT, Cambridge, Mass., 1977.
16. C. MOOERS AND A. R. ROBINSON, "Report of the Ocean Prediction Workshop, 1981," Naval Postgraduate School, Monterey, Calif., 1981.
17. W. B. OWENS, *J. Phys. Oceanogr.* **9** (1979), 337.
18. W. B. OWENS AND F. B. BRETHERTON, *Deep-Sea Res.* **25** (1978), 1.
19. J. G. RICHMAN, "Kinematics and Energetics of the Mesoscale Mid-Ocean Circulation: MODE," Ph.D. Thesis, MIT/WHOI, Cambridge, Mass., 1976.
20. A. R. ROBINSON, Dynamics of Ocean Currents and Circulation: Results of POLYMODE and Related Investigations, *in* "Proceedings of the International School of Physics, Summer Institute, Varenna, Italy, 1980;" preprinted as POLYMODE Report, December 1980, USPMOC-MIT.
21. A. R. ROBINSON, D. E. HARRISON, AND D. B. HAIDVOGEL, *Dyn. Atmos. Oceans* **3** (1979), 143.
22. A. R. ROBINSON AND D. B. HAIDVOGEL, *J. Phys. Oceanogr.* **10** (1980), 1909.
23. R. SHAPIRO, *Rev. Geophys. Space Phys.* **8** (1970), 359.